Physics Letters B 779 (2018) 214–222

Contents lists available at ScienceDirect

Physics Letters B

www.elsevier.com/locate/physletb

# On extremal surfaces and de Sitter entropy

K. Narayan

*Chennai Mathematical Institute, SIPCOT IT Park, Siruseri 603103, India*

ARTICLE INFO

*Article history:*
Received 15 November 2017
Received in revised form 23 January 2018
Accepted 7 February 2018
Available online 12 February 2018
Editor: N. Lambert

ABSTRACT

We study extremal surfaces in the static patch coordinatization of de Sitter space, focusing on the future and past universes. We find connected timelike codim-2 surfaces on a boundary Euclidean time slice stretching from the future boundary $I^+$ to the past boundary $I^-$. In a limit, these surfaces pass through the bifurcation region and have minimal area with a divergent piece alone, whose coefficient is de Sitter entropy in 4-dimensions. These are reminiscent of rotated versions of certain surfaces in the $AdS$ black hole. We close with some speculations on a possible $dS/CFT$ interpretation of 4-dim de Sitter space as dual to two copies of ghost-CFTs in an entangled state. For a simple toy model of two copies of ghost-spin chains, we argue that similar entangled states always have positive norm and positive entanglement.



## 1. Introduction

de Sitter space is fascinatingly known to have temperature and entropy [1]: see e.g. [2] for a review. This is most easily seen in the static patch coordinatization of de Sitter space $dS_{d+1}$,

$$ds^2 = -\left(1-\frac{r^2}{l^2}\right)dt^2 + \frac{dr^2}{1-\frac{r^2}{l^2}} + r^2 d\Omega_{d-1}^2 \,, \tag{1.1}$$

as we review in sec. 2. The Penrose diagram in Fig. 1 represents the $(t,r)$-plane: each point is an $S^{d-1}$. The static patches refer to the Northern and Southern hemisphere regions $N$ and $S$ where $t$ is a timelike coordinate and time translations are Killing isometries. $N$ and $S$ have $0 \le r \le l$, with $r=0$ the Poles and $r=l$ the cosmological horizon. In the future and past universes $F$ and $P$, $t$ is a spacelike direction and $r$ becomes time so constant $r$ surfaces are spacelike.

de Sitter entropy is essentially the area of the cosmological horizon, apparently stemming from degrees of freedom not accessible to observers in regions $N$ and $S$, for whom the horizons are event horizons. It is of interest to understand if this entropy can be realized in gauge/gravity duality [3–6] for de Sitter space or $dS/CFT$ [7–9] which associates de Sitter space to a dual nonunitary Euclidean CFT on the future (or past) boundary. In particular one might wonder if de Sitter entropy is encoded in some generalization of the holographic formulation of entanglement entropy [10–13] via the areas of appropriate extremal surfaces.

In ordinary (static) quantum systems, we consider spatial subsystems on a constant time slice and entanglement entropy then arises by a partial trace over the environment. Towards mimicking this in the dual Euclidean CFT here, extremal surfaces on a constant boundary Euclidean time slice were studied in [14,15]: these are anchored at the future boundary $I^+$ in the upper Poincare patch of de Sitter space and dip into the bulk time direction. Real extremal surfaces are either null with (minimal) vanishing area or timelike with maximal area stemming from a divergent term alone. However the areas of certain complex codim-2 extremal surfaces (involving an imaginary bulk time parametrization) were found to have structural resemblance with entanglement entropy in the dual Euclidean CFT for the upper patch (defined in terms of some boundary Euclidean time direction): in $dS_4$, these areas are negative, consistent with the negative central charge [9] in $dS_4/CFT_3$. These end up being equivalent to analytic continuation from the Ryu–Takayanagi expressions in $AdS/CFT$. Further investigations [16–18] study generalizations of entanglement entropy for theories with negative norm states, in particular ghost systems.

The present static patch coordinatization of de Sitter space, Fig. 1, raises the possibility of de Sitter entropy arising from the area of appropriate connected extremal surfaces stretching from the boundary of some subregion at the future boundary $I^+$ of $F$ to some equivalent subregion at the past boundary $I^-$ of $P$. Naively this might then allow an interpretation of the surface as representing some "generalized entanglement" between the future and past copies of the Euclidean CFT. These are reminiscent of certain surfaces studied by Hartman and Maldacena [19] in the $AdS$ black hole, except the present surfaces stretching in the time direction between $I^+$ and $I^-$ are in some sense rotated versions thereof

*E-mail address:* narayan@cmi.ac.in.

https://doi.org/10.1016/j.physletb.2018.02.010

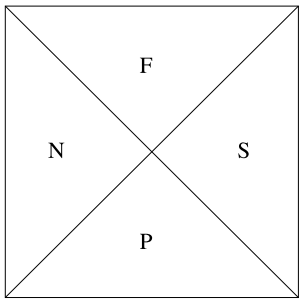


**Fig. 1.** Penrose diagram of de Sitter space in static coordinates: $N$ and $S$ are the Northern and Southern hemispheres. $F$ and $P$ are future and past universes.

(similar surfaces were in fact studied in [14] in the de Sitter bluewall [20] as we discuss below).

We review the static patch and de Sitter entropy in sec. 2 and a version of entanglement as interface area. In sec. 3, we describe extremal surfaces in $F$ and $P$: we find that 4-dim de Sitter entropy $\frac{l^2 V_{S^2}}{4G_4} = \frac{\pi l^2}{G_4}$ arises as the coefficient of the divergent area of certain connected codim-2 real timelike extremal surfaces lying in a boundary Euclidean time slice of the bulk space, stretching from $I^+$ to $I^-$. These pass through the bifurcation region and have minimal area. It is worth noting that the horizons from the point of view of $F$ and $P$ are not event horizons but Cauchy horizons, so that this recovery of de Sitter entropy might appear unconventional. We close with some speculations (sec. 4) on a $dS/CFT$ interpretation of $dS_4$ as dual to two copies of ghost-CFTs on $I^+$ and $I^-$ in particular entangled states. Appendices A, B review aspects of Poincare $dS$ extremal surfaces and ghost-spins.

## 2. The static patch and de Sitter entropy

The Euclidean continuation $t \to -it_E$ of (1.1) gives $ds_E^2 = \frac{dr^2}{1-r^2/l^2} + (1-\frac{r^2}{l^2})dt_E^2 + r^2 d\Omega_{d-1}^2$ which is a sphere, and de Sitter entropy can be obtained as for black holes. Regularity requires that there be no conical singularity in the $(t,r)$-plane at the origin (which was the location of the horizon). This makes $t_E$ an angular variable with periodicity $2\pi l$ which is the inverse Hawking temperature of de Sitter space. With the horizon as one boundary, the Euclidean action gives

$$I_E = -\int \frac{r^{d-1} dr dt_E d\Omega_{d-1}}{16\pi G_{d+1}} \left(R - \frac{d(d-1)}{l^2}\right) = -\frac{V_{S^{d-1}}(2\pi l)}{16\pi G_{d+1}} \frac{2d}{l^2} \frac{r^d}{d}\Big|_0^l = -\frac{l^{d-1} V_{S^{d-1}}}{4G_{d+1}} . \tag{2.1}$$

Equivalently, the Euclidean continuation of $dS_{d+1}$ is $S^{d+1}$ with $ds^2 = l^2 ds_{S^{d+1}}^2$: this gives $I_E = -\int \frac{d\Omega_{d+1} l^{d+1}}{16\pi G_{d+1}} \frac{2d}{l^2}$ using $V_{S^d} = \frac{2\pi^{(d+1)/2}}{\Gamma((d+1)/2)}$ and $V_{S^{d+1}} = \frac{2\pi}{d} V_{S^{d-1}}$. Since the sphere has no boundary, there is no "energy" contribution to $I_E$ so $E = 0$, giving

$$\log Z = -\beta F = -\beta E + S = -I_E \quad \Rightarrow \quad S_{dS_{d+1}} = -I_E = \frac{l^{d-1} V_{S^{d-1}}}{4G_{d+1}} , \tag{2.2}$$

giving the entropy of de Sitter space. For $dS_4$, this is $S_{dS_4} = \frac{\pi l^2}{G_4}$.

Since the regions $N$ and $S$ are static with $t$-translations being isometries, it is natural to ask if there are extremal surfaces which wrap the horizon in the IR limit and whose area recovers de Sitter entropy. We recall that in the $AdS$ black brane, the Ryu–Takayanagi minimal surface [10] wraps the horizon in the IR limit where the subsystem approaches the full space and the finite part of entanglement entropy given by the minimal surface area approaches the entropy of the black brane given by the horizon area. Thus consider a constant time slice $t = const$: the spatial metric is

$$d\sigma^2 = \frac{dr^2}{1-r^2/l^2} + r^2 d\Omega_{d-1}^2 = l^2(d\theta^2 + \sin^2\theta d\Omega_{d-1}^2) , \tag{2.3}$$

where the Southern hemisphere has $r = l\sin\theta$ with $0 \le r \le l$ so $0 \le \theta \le \frac{\pi}{2}$ and likewise for the Northern hemisphere. Thus the $t = const$ slice of the static patch is a sphere comprising two hemispheres with $r$ the latitudinal coordinate. The horizons at $r^2 = 1$ are then the equators at the boundary $\theta = \frac{\pi}{2}$ of the hemisphere (with the Poles at $r = 0$ or $\theta = 0$). Notably, unlike $AdS$, the coordinate $r$ is not a bulk radial coordinate but simply an angular direction on the hemisphere (which has no boundary): latitudes at $r = const$ define hemispherical caps which might be the most natural subsystems here.

Each latitude divides the full sphere into the subsystem and the rest of the sphere (which comprises the rest of the hemisphere containing the cap and the other hemisphere). It is intuitive to define the entanglement entropy as the interface area in Planck units. The latitude defined by the equator at $r = l$ divides the full sphere into a subsystem defined by one hemisphere and the environment which is the other hemisphere. Then the entanglement entropy between the two hemispheres becomes de Sitter entropy,

$$S_r = \frac{r^{d-1} V_{S^{d-1}}}{4G_{d+1}} \quad \to \quad \frac{l^{d-1} V_{S^{d-1}}}{4G_{d+1}} . \tag{2.4}$$

In this limit, the interface is in fact the horizon, and so this agrees with the familiar statement that de Sitter entropy is the area of the cosmological horizon in Planck units. See also e.g. [21], [22].

## 3. The future and past universes and extremal surfaces

The future and past de Sitter universes in (1.1) with $1 \le \frac{r}{l} \le \infty$ can be described as

$$ds^2 = \frac{l^2}{\tau^2}\left(-\frac{d\tau^2}{1-\tau^2} + (1-\tau^2)dw^2 + d\Omega_{d-1}^2\right), \quad \tau = \frac{l}{r} , \quad w = \frac{t}{l} . \tag{3.1}$$

$\tau$ is now the "bulk" time coordinate while $w$ is a spatial coordinate enjoying translation invariance. The maximal extension encoded in the Penrose diagram exhibits horizons at $\tau = 1$, which are Cauchy horizons for the future and past universes $F$ and $P$. For instance there are trajectories which end in $N$ or $S$ so they cannot be part of the Cauchy data whose time development leads to $I^+$: thus the future horizons are past Cauchy horizons for data on $I^+$ acting as causal boundaries for the future universe $F$ cloaking the static patches. Likewise the past horizons are future Cauchy horizons for Cauchy data on $I^-$ (related discussions appear in the de Sitter bluewall [20]). The future and past boundaries $I^+$ and $I^-$ are at $\tau = 0$. The asymptotic structure of the future universe is

$$\frac{r}{l} \gg 1: \quad ds^2 \sim -l^2\frac{dr^2}{r^2} + \frac{r^2}{l^2}dt^2 + r^2 d\Omega_{d-1}^2 \sim \frac{l^2}{\tau^2}\left(-d\tau^2 + dw^2 + d\Omega_{d-1}^2\right) . \tag{3.2}$$

This is akin to the Poincare patch of de Sitter space except that the boundary is not $R^d$ but Euclidean $R \times S^{d-1}$. This is analogous to global $AdS_{d+1}$ where the boundary is $R_{time} \times S^{d-1}$. Constant $\tau$ slices (i.e. $r = const$ slices in (1.1)) have topology $R \times S^{d-1}$.

We want to look for extremal surfaces stretching from $I^+$ to $I^-$ whose area might capture de Sitter entropy. The scaling $\frac{l^{d-1}}{G_{d+1}}$ of de Sitter entropy suggests that the surfaces in question are codimension-2. From the point of view of entanglement in the dual theory defined with respect to Euclidean time, it would seem reasonable to look for bulk surfaces lying on an appropriately defined constant boundary Euclidean time slice of the bulk space. Noting that the space enjoys $t$-translation symmetry as well as rotational invariance in $S^{d-1}$, let us imagine restricting to (i) an equatorial plane of the $S^{d-1}$, or (ii) a $t = const$ surface as a constant boundary Euclidean time slice.

### 3.1. An $S^{d-1}$ equatorial plane

We restrict to an equatorial plane with $\theta = \frac{\pi}{2}$. The rotational symmetry implies that all such equatorial planes are equivalent. The metric on such a slice from (3.1) is

$$ds^2 = -\frac{l^2}{\tau^2}\left(\frac{d\tau^2}{1-\tau^2} + (1-\tau^2)dw^2 + d\Omega_{d-2}^2\right) . \tag{3.3}$$

This equatorial slice can be thought of as follows: the future component comprises a family of concentric cylinders $R_w \times S^{d-2}$ at $\tau = const$ slices, with size $\frac{l}{\tau}$ and $\tau$ representing the radial direction, the outermost cylinder having size $\frac{l}{\epsilon}$ while the innermost has size $l$. The past component comprises a similar family with $\tau$ again running over $l \le \tau \le \frac{l}{\epsilon}$. The two join at the bifurcation region (the intersection of the horizons) with $\tau = 1$: this is a smooth $S^{d-2}$ as can be seen via Kruskal-type coordinates with $y$ the "tortoise" coordinate

$$u = e^{w-y}, \quad v = -e^{-w-y}, \quad y = \int \frac{dr}{1-\tau^2} = \frac{1}{2}\log\left|\frac{1+\tau}{1-\tau}\right| \\ [0 < \tau < \infty] . \tag{3.4}$$

We want to impose boundary conditions that reflect extremal surfaces stretching from the boundary of a subsystem of the form $\Delta w \times S^{d-2}$ at $I^+$ dipping into the bulk, to finally end at the boundary of an equivalent subsystem at $I^-$, as in Fig. 2. These could either penetrate the horizons somewhere, or pass through the bifurcation region without intersecting the horizons (as do all static observers at any fixed $w$). With $\frac{dw}{d\tau} \equiv w'$, the area functional is

$$S = l^{d-1} V_{S^{d-2}} \int \frac{d\tau}{\tau^{d-1}} \sqrt{\frac{1}{1-\tau^2} - (1-\tau^2)(w')^2} . \tag{3.5}$$

The subsystems in question are on $I^+/I^-$ and so spacelike: we therefore take these to be real surfaces orthogonal to the subsystems and so timelike at least initially (i.e. $w' \sim 0$ near the boundary $\tau = 0$ and $S \sim \int l^{d-1}\frac{d\tau}{\tau^{d-1}}$), thereby choosing the sign under the square root. Along the lines of the de Sitter bluewall [20] analysed in [14], we obtain

$$\frac{-(1-\tau^2)w'}{\sqrt{\frac{1}{1-\tau^2} - (1-\tau^2)(w')^2}} \frac{1}{\tau^{d-1}} = B \\ \Rightarrow \quad \frac{1}{1-\tau^2} - (1-\tau^2)(w')^2 = \frac{1}{1-\tau^2+B^2\tau^{2d-2}} , \tag{3.6}$$

giving ($I^\pm$ are regulated at $\epsilon$, and $\tau_*$ is the turning point discussed below)

$$\dot{w}^2 \equiv (1-\tau^2)^2(w')^2 = \frac{B^2\tau^{2d-2}}{1-\tau^2+B^2\tau^{2d-2}} ,$$

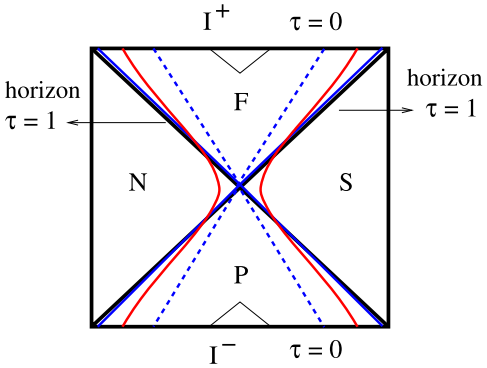


**Fig. 2.** Timelike extremal surfaces in the $(\tau, w)$-plane stretching from $I^+$ to $I^-$. These are akin to rotated versions of the surfaces of Hartman–Maldacena in the $AdS$ black hole. The red timelike surface intersects the horizons. The limiting blue surface is almost null (almost hugging the horizons) and passes through the bifurcation region: it has minimal area. (For interpretation of the references to colour in this figure legend, the reader is referred to the web version of this article.)

$$S = 2l^{d-1} V_{S^{d-2}} \int_\epsilon^{\tau_*} \frac{d\tau}{\tau^{d-1}} \frac{1}{\sqrt{1-\tau^2+B^2\tau^{2d-2}}} . \tag{3.7}$$

Here $B$ is a conserved constant. The factor of 2 in the area arises because we are calculating the areas for both the top and bottom half-surfaces (see Fig. 2). The structure of these extremal surfaces is somewhat different from those in the Poincare slicing [14] (reviewed briefly in Appendix A): for sufficiently small subsystems however, (3.7) approaches (A.2).

In (3.7), $\dot{w} = (1-\tau^2)\frac{dw}{d\tau}$ is the $y$-derivative with $y$ in (3.4) above, useful in the vicinity of the horizons. Near the boundary $\tau \to 0$, we have $\dot{w} \to 0$ for any nonzero finite $B$: further we have $\dot{w} < 1$ for $\tau < 1$ (within the future universe), i.e. the surface drops down towards the past. As $\tau \to 1$, we have $\dot{w} \to 1$, i.e. the surface grazes the horizon (is tangent to the horizon) when it intersects the horizon. $\tau > 1$ gives $\dot{w} > 1$: this is in the regions $N$ or $S$, after crossing the horizon. Note that $\tau = const$ surfaces within $N$ or $S$ are timelike.

The turning point $\tau_*$ is the "deepest" location to which the surface dips into in the bulk, before turning around: this is when $\dot{w} \to \infty$ or $\frac{dy}{dw} = 0$. Thus the surface has no variation in the $\tau$- (or $y$-)direction, i.e. it is tangent to $\tau = const$ curves at the location $\tau_*$ (see the red curve in Fig. 2). From (3.7), we see that for $\tau < 1$ (within $F$ or $P$), the surface has no tendency to turn around since $\dot{w} < 1$: however the surface can have a turning point if $\tau > 1$. To see this explicitly, we note using (3.4) in (3.7) that

$$\tau > 1: \qquad \dot{w}^2 = \left(\frac{dw}{dy}\right)^2 = 1\Big/\left(1 - \frac{4e^{2y}(e^{2y}-1)^{2d-4}}{B^2(e^{2y}+1)^{2d-2}}\right) . \tag{3.8}$$

$y \to \infty$ at the $\tau = 1$ horizons and $\dot{w}^2 \to 1$ i.e. $w \to \pm y$ (the area functional (3.5) recast using the Kruskal coordinates $u, v$ in (3.4) can be seen to be regular at the $\tau = 1 = \frac{1-uv}{1+uv}$ horizons, i.e. $u = 0$ or $v = 0$). The turning point is at

$$|\dot{w}| \to \infty: \qquad 1 - \tau_*^2 + B^2\tau_*^{2d-2} = 0 = 1 - \frac{4e^{2y_*}(e^{2y_*}-1)^{2d-4}}{B^2(e^{2y_*}+1)^{2d-2}} . \tag{3.9}$$

At $\tau_*$, the surface from $I^+$ is joined with the surface from $I^-$. We have $w \sim \sqrt{\tau_* - \tau}$ from above (near $\tau \lesssim \tau_*$) joining $w \sim -\sqrt{\tau_* - \tau}$ from below smoothly. This gives the full smooth "hourglass"-shaped surfaces in Fig. 2. Thus the surface starts at $w = \pm\frac{\Delta w}{2}$ on $I^+$, intersects the future horizons at $\tau = 1$, $w = \pm\infty$,

turns around at $\tau_*$ in $N/S$, then intersects the past horizons at $\tau = 1$, $w = \mp\infty$, finally reaching $w = \mp\frac{\Delta w}{2}$ on $I^-$.

We will now mostly focus on 4-dim de Sitter space $dS_4$ (i.e. $d = 3$) which turns out to be most interesting. From (3.7), since $1 - \tau^2 + B^2\tau^4 = (1 - B\tau^2)^2 + (2B - 1)\tau^2$, we have

$$0 < B < \frac{1}{2}: \quad \dot{w} \to \infty\,, \qquad 1 - \tau_*^2 + B^2\tau_*^4 = 0\,, \tag{3.10}$$

giving the turning point $\tau_*(B^2)$ as a function of the parameter $B^2$. For $B = 0$, we have $\tau_* = 1$: small $B$ gives $\tau_* \gtrsim 1$. The limit $B \to 0$ gives $\tau_* \to 1$, i.e. the surface mostly remains in $F$ (or $P$), penetrating the horizon close to the bifurcation region, to finally turn around at

$$\tau_* = 1 + \delta \quad \Rightarrow \quad -2\delta + B^2 \sim 0 \sim 1 - \frac{4}{B^2 e^{2y_*}} \quad \Rightarrow \quad \delta \sim \frac{B^2}{2}\,. \tag{3.11}$$

So $\delta \to 0$ as $B \sim 0$: these approach "maximally timelike" surfaces stretching only in the bulk time direction with $\dot{w} \sim 0$. From (3.7), the area for $B = 0$ in Planck units becomes

$$\frac{S}{4G_{d+1}} = \frac{2l^{d-1}V_{S^{d-2}}}{4G_{d+1}} \int_\epsilon^1 \frac{d\tau}{\tau^{d-1}} \frac{1}{\sqrt{1-\tau^2}}\,. \tag{3.12}$$

The surface stretches from the boundary $\tau = \epsilon$ in the future universe to the bifurcation region with $\tau_* = 1$ and then has a similar piece in the past universe. For $dS_4$, the surface is a 1-dimensional curve in the $(\tau, w)$-plane and wraps the $S^1$ on a $\tau = const$ slice. This gives

$$\frac{S}{4G_4} = \frac{2l^2(2\pi)}{4G_4}\left(\frac{-\sqrt{1-\tau^2}}{\tau}\right)\Big|_\epsilon^1 = \frac{\pi l^2}{G_4}\frac{l}{\epsilon_c}, \quad [\epsilon_c = l\epsilon] \tag{3.13}$$

The coefficient of this divergent area in Planck units is precisely de Sitter entropy. The bulk surface stretches from the future boundary $I^+$ regulated at $\epsilon = \frac{\epsilon_c}{l}$ (expressed in terms of the de Sitter scale $l$), and passes through the bifurcation region at $\tau = 1$. The turning point is contained in the bifurcation region, and so is fixed at $\tau_* = 1$. Interpreting this as an area law divergence in a dual CFT however, rescaling the ultraviolet cutoff changes the precise coefficient.

### 3.2. Features of $S^{d-1}$ equatorial plane extremal surfaces

In general, de Sitter space does not appear to exhibit interesting solutions to extremization, unlike $AdS$: e.g. in the Poincare slicing (which is the local geometry near any point at $I^+$), as we have mentioned earlier, surfaces do not have any real turning point, reviewed briefly in Appendix A (complex extremal surfaces were found in [14] which amount to analytic continuation from Ryu–Takayanagi in $AdS$). The surfaces (3.7) circumvent this since they stretch from $I^+$ to $I^-$: these surfaces are somewhat special, as we discuss below.

Firstly, it is interesting to note that the subsystem size does not enter in (3.12), (3.13), at all. In particular in the limit as the subsystem size becomes the entire space $\Delta w \to \infty$, the smooth red curve in Fig. 2 becomes the limiting blue curve as $B \to 0$. This surface has $\tau_* \to 1$ and hugs the horizons without intersecting them: it just grazes the future horizon dropping down from $I^+$, and then smoothly turns around and hugs the past horizon to eventually hit $I^-$. The surface thus appears to exclude precisely the regions behind the horizons, i.e. regions $N, S$, restricted to this equatorial plane.

These $B = 0$ surfaces passing through the bifurcation region in fact have minimal area. Firstly we mention that this is confirmed by numerical evaluation of the area integral in (3.7). Secondly, in the neighbourhood of $B = 0$, we can also analytically evaluate the change in the area: with $S = \int_\epsilon^{\tau_*(B^2)} L(\tau, B^2)d\tau$, we have the first order change for infinitesimal $\delta B^2$,

$$\delta S = \Big( \int_\epsilon^{\tau_*(B^2)} \frac{\partial L}{\partial B^2}(\tau_*(B^2))d\tau + L(\tau_*(B^2), B^2)\frac{\partial \tau_*(B^2)}{\partial B^2}\Big)\,\delta B^2\,. \tag{3.14}$$

For the $dS_4$ surfaces in (3.12), (3.13) with $B^2 = 0$, turning on a small $\delta B^2$ and using (3.11), we find that a term singular near $\tau_* = 1$ cancels between both terms in $\delta S$ giving $\delta S = \frac{\pi}{2}\delta B^2 > 0$. Thus the deformation (3.11) of the $B = 0$ surface increases its area.

More broadly, for any $B > \frac{1}{2}$ we see that $1 - \tau^2 + B^2\tau^4 = (1 - B\tau^2)^2 + (2B - 1)\tau^2 > 0$ does not vanish: thus there is no turning point solution to (3.10). The value $B = \frac{1}{2}$ in $dS_4$ gives $\dot{w}^2 = \frac{\tau^4/4}{(1-\tau^2/2)^2}$. Thus at this special value of $B$, the turning point is at $\tau_* = \sqrt{2}$ where $\dot{w} \to \infty$ with a double zero in the denominator. The subregion width $\Delta w$ acquires a divergence near $\tau_* = \sqrt{2}$: the surface area also has a logarithmic divergence here. There is an accumulation of surfaces with turning point near $\tau_* = \sqrt{2}$ which is a limiting value: the surfaces appear to be "repelled" from dipping into the static patches $N$ or $S$ to larger $\tau_*$ values. For generic $0 < B < \frac{1}{2}$, the turning point is given by a single zero of the polynomial in (3.10): of the two positive roots, we pick the root satisfying $\tau_* < \sqrt{2}$ which is the limiting value. For $B > \frac{1}{2}$ extremal surfaces stretching from $I^+$ to $I^-$ do not exist: there are however e.g. disconnected null surfaces with $B \to \infty$ lying entirely within $F$ (or $P$) as shown by the small disconnected black wedges in Fig. 2.

Thus for any given subsystem $(\Delta w \times S^1)^2 \in I^+ \cup I^-$, we finally see that there are:

- minimal (zero) area disconnected surfaces with $B \to \infty$: from (3.7), these are null with $\dot{w} = 1$ and vanishing area, shown as the two disconnected black wedges in Fig. 2. Each wedge is seen to have support only at one boundary ($I^+$ or $I^-$): with $B$ large, the area in (3.7) is $S \sim 2l^{d-1}V_{S^{d-2}}\int_\epsilon^{\tau_*} \frac{d\tau}{\tau^{d-1}} \frac{1}{\sqrt{1+B^2\tau^{2d-2}}}$, and we see that there is no smooth turning point. The black wedges are real null surfaces with $S \to 0$ as $B \to \infty$ (half-surfaces joined with a cusp at $\tau_*$, similar to the real null surfaces in [14]). Sufficiently small subregions can be approximated as akin to the flat Poincare slicing, as is clear from the area approximation here, and so also admit complex extremal surface solutions as in [14] with negative area.
- minimal area connected surfaces with $B = 0$ and area (3.12), (3.13): for generic $\Delta w$, these are shown as the dotted blue lines from $I^+$ to $I^-$, with the limiting blue curve for $\Delta w \to \infty$ cloaking the horizons. From (3.7), we see that these surfaces simply "hang down" from $I^+$ till $I^-$ without bending or turning since $\dot{w} = 0$. The area is independent of the size of the subregion for these surfaces, which all pass through the bifurcation region. The surfaces with infinitesimal $B$ in (3.11) which intersect the horizons with a smooth turning point just inside the horizon asymptote to these $B = 0$ surfaces. The area in (3.7) smoothly asymptotes to (3.12), (3.13), as $B \to 0$ and is then minimal. These surfaces are reminiscent of the surfaces of Hartman–Maldacena [19] in the $AdS$ black hole: perhaps this is not surprising since in some sense the de Sitter static patch coordinatization is a rotation of $AdS$ (although not an analytic continuation).

Overall, for $B$ small, the term with the minus sign dominates over the $B^2$-term under the square root so that the area integral in (3.7) (approaching (3.12)) bears resemblance to the Ryu–Takayanagi area integral $S = 2R^{d-1}V_{d-2}\int_\epsilon^{r_*}\frac{dr}{r^{d-1}}\frac{1}{\sqrt{1-r^{2d-2}/r_*^{2d-2}}}$ with $r_* \sim l$ for a strip subsystem of width $l$ in $AdS$: the full integral in fact has some similarity to the area integrals for strip subsystems in the $AdS$ plane wave geometry [23]. In some sense, the neighbourhood of the bifurcation region in the static $dS$ patch behaves like $AdS$ with regard to the area functional extremization.[1] This singles out these minimal area connected surfaces above in de Sitter space as special.

For other dimensions, the coefficient scales as $dS$ entropy but is not precisely that:

$$[dS_3]\ \ \frac{S}{4G_3} = \frac{2.2l}{4G_3}\int_\epsilon^1 \frac{d\tau}{\tau}\frac{1}{\sqrt{1-\tau^2}} = \frac{l}{G_3}\log\frac{2}{\epsilon}\ ;$$
$$[dS_5]\ \ \frac{S}{4G_5} = \frac{\pi l^3}{G_5}\left(\frac{1}{\epsilon^2}+\log\frac{2}{\epsilon}\right). \tag{3.15}$$

This is not surprising: the surface in (3.12) wraps an $S^{d-2}$ and the horizon directions in the $(\tau, w)$-plane, which compensates precisely for the $S^{d-1}$ in (2.2) only for $dS_4$ interestingly.

These surfaces bear some qualitative similarity to the trajectories of timelike geodesics stretching from $I^+$ to $I^-$ in the $(\tau, w)$-plane. A $w = const$ timelike geodesic in the $(\tau, w)$-plane is a straight line passing through the bifurcation region. In general, timelike geodesics have action $S = \int\sqrt{-g_{\tau\tau}d\tau^2 + g_{ww}dw^2}$. Simplifying, we see that this is identical to (3.5) with $d = 2$: thus the length of such limiting geodesics is similar to the $dS_3$ result above. Likewise for codim-1 surfaces, the area functional $S = l^d V_{S^{d-1}}\int\frac{d\tau}{\tau^d}\sqrt{\frac{1}{1-\tau^2}-(1-\tau^2)(w')^2}$ can be seen to scale as $l^d$ in $dS_{d+1}$. Analysing this shows that codim-1 surfaces with $B = 0$ in $dS_4$ have $S = 2l^3V_{S^2}\int_\epsilon^1\frac{dr}{r^3}\frac{1}{\sqrt{1-r^2}} = 4\pi l^3(\frac{1}{\epsilon^2}+\log\frac{2}{\epsilon})$.

### 3.3. The $w = const$ slice

From (3.1), the metric on this slice becomes

$$ds^2 = -l^2\frac{d\tau^2}{\tau^2(1-\tau^2)} + \frac{l^2}{\tau^2}(d\theta^2 + \sin^2\theta d\Omega_{d-2}^2)\ . \tag{3.16}$$

All $w = const$ slices pass through the bifurcation region. The natural subsystem here is a cap-like region defined by a latitude at $\theta = const$ on the $S^{d-1}$ at the future boundary. The extremal surface we are looking for stretches from the boundary of one such cap at $I^+$ to an equivalent cap on the $S^{d-1}$ at the past boundary $I^-$, as in Fig. 3. Both caps wrap an $S^{d-2}$ on the $S^{d-1}$. The area functional is

$$S = 2\int\frac{l^{d-1}V_{S^{d-2}}(\sin\theta)^{d-2}}{\tau^{d-1}}\sqrt{\frac{d\tau^2}{1-\tau^2}-d\theta^2}$$
$$= 2l^{d-1}V_{S^{d-2}}\int\frac{d\tau}{\tau^{d-1}}(\sin\theta)^{d-2}\sqrt{\frac{1}{1-\tau^2}-(\theta')^2}\ . \tag{3.17}$$

The factor of 2 arises as before from the two components of the surface, one stretching from $I^+$ and another from $I^-$. The equation of motion $\frac{d}{d\tau}(\frac{\partial L}{\partial\theta'}) = \frac{\partial L}{\partial\theta}$ becomes

[1] While the Poincare slicing (Appendix A) must also exhibit these as geometric surfaces, they appear tricky to see directly.

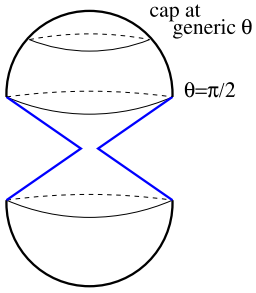


**Fig. 3.** Timelike extremal surfaces in the $(\tau, \theta)$-plane stretching from $\mathcal{I}^+$ to $\mathcal{I}^-$. The limiting blue surface stretches from one hemisphere ($\theta = \frac{\pi}{2}$) at $I^+$ to another equivalent one at $I^-$. (For interpretation of the references to colour in this figure legend, the reader is referred to the web version of this article.)

$$\frac{d}{d\tau}\left(\frac{-\theta'}{\sqrt{\frac{1}{1-\tau^2}-(\theta')^2}}\frac{(\sin\theta)^{d-2}}{\tau^{d-1}}\right)$$
$$= (d-2)\frac{(\sin\theta)^{d-3}}{\tau^{d-1}}\cos\theta\sqrt{\frac{1}{1-\tau^2}-(\theta')^2}\ . \tag{3.18}$$

The analogs of the extremal surfaces earlier passing through the bifurcation region with $w' = 0$ in this case are surfaces which "hang" down into the bulk without turning, i.e. with $\theta' = 0$. (By contrast, $\theta'$ maximum gives $\theta' = \frac{1}{\sqrt{1-\tau^2}}$, which are null surfaces with vanishing (minimal) area.) With $\theta' = 0$, we see from (3.18) that a surface "hanging down" at generic $\theta = const$ is not extremal: although the left hand side of (3.18) vanishes, the right hand side does not. However we are most interested in the limit where the subregion is maximal, i.e. when the cap-like region becomes the entire hemisphere on the $S^{d-1}$: this is when $\theta = \frac{\pi}{2}$. It can be seen that this now is a solution to the extremization equation above: the right hand side vanishes with $\cos\frac{\pi}{2} = 0$. For these limiting surfaces, the area becomes

$$\theta = \frac{\pi}{2}:\ \ \frac{S}{4G_{d+1}} = \frac{2l^{d-1}V_{S^{d-2}}}{4G_{d+1}}\int_\epsilon^1\frac{d\tau}{\tau^{d-1}}\frac{1}{\sqrt{1-\tau^2}} \xrightarrow{dS_4} \frac{\pi l^2}{G_4}\frac{1}{\epsilon}\ . \tag{3.19}$$

Thus this again recovers de Sitter entropy as the coefficient of the area law divergence as in the previous case (3.12), (3.13). The geometry of these surfaces away from precisely $\theta' = 0$ is however somewhat different. This can be seen in some detail in the $dS_3$ case, i.e. $d = 2$. Since $\theta$ is now a cyclic coordinate in (3.17), we have a conserved quantity $A = \frac{\partial L}{\partial\theta'}$ giving

$$\theta' = \frac{A\tau}{\sqrt{(1-\tau^2)(1+A^2\tau^2)}}\ . \tag{3.20}$$

For $A \to \infty$, these are null surfaces

$$\theta' = 1/\sqrt{1-\tau^2}\ \ \Rightarrow\ \ \tau = \sin(\theta_0-\theta)\ ;$$
$$\tau_{max} = \sin\theta_0\ \to\ 1\ \text{ as }\ \theta_0 \to \pi/2\ . \tag{3.21}$$

These are disconnected surfaces with (minimal) vanishing area. For precisely $A = 0$, these are $\theta = const$ surfaces which "hang down" into the bulk without turning, but slightly different geometrically from the ones in the equatorial plane earlier: to see this, consider small $A = \varepsilon$ and $\theta_0 = \frac{\pi}{2}$. Then as $\tau \to 1$, we have

$$\theta' \sim \pm A\tau/\sqrt{1-\tau^2} \qquad \Rightarrow \qquad \theta - \theta_0 \sim \pm A\sqrt{2(1-\tau)}\ . \tag{3.22}$$

We see that for any nonzero infinitesimal $A$, the surface at $\theta \sim \theta_0$ has a tendency to turn as $\tau \to 1 - O(A^2)$ with $\theta' \to \infty$. However $\theta$ is essentially constant till very near $\tau = 1$ and then $\theta - \theta_0 \sim O(A) \sim O(\varepsilon)$. Thus these surfaces at $\theta = \frac{\pi}{2}$ stretch from $I^+$ to $\tau \sim 1$ where they acquire an $O(A)$ "dimple" where $\theta' \to \infty$. The full connected surface (after joining an equivalent surface from $I^-$ in $P$) thus has an $O(A)$ constriction at the neck in Fig. 3, and so is not smooth unlike the $\theta' = 0$ surface at $\theta = \frac{\pi}{2}$ (or the red curves in Fig. 2).

For other dimensions, it appears difficult to identify exact solutions although they may well exist. Null surfaces of course continue to arise as in (3.21). Considering $\theta' = 0$ surfaces, let us now consider the neighbourhood of the $\theta = \frac{\pi}{2}$ extremal surface: parametrizing this as $\theta(\tau) = \frac{\pi}{2} - \delta\theta(\tau)$ to $O(\delta\theta)$ gives $\cos\theta \sim \delta\theta(\tau)$ and the linearized equation

$$\frac{d}{d\tau}\left(\frac{-\sqrt{1-\tau^2}}{\tau^{d-1}}\,\frac{d\delta\theta(\tau)}{d\tau}\right) = \frac{d-2}{\tau^{d-1}}\,\frac{\delta\theta(\tau)}{\sqrt{1-\tau^2}}\,. \tag{3.23}$$

The solution that is regular as $\tau \to 0, 1$, and in addition exhibits $\theta'$ monotonically increasing till $\theta' \to \infty$ as $\tau \to 1$ is $\delta\theta(\tau) = \tau^d\ {}_2F_1\big(\frac{1+d-\sqrt{d^2+2d-7}}{4}, \frac{1+d+\sqrt{d^2+2d-7}}{4}, 1+\frac{d}{2};\ \tau^2\big)$, involving the hypergeometric function ${}_2F_1$. Since $\delta\theta(\tau)$ encodes the infinitesimal linearization about $\theta = \frac{\pi}{2}$, regularity of this solution implies that the surface $\theta(\tau)$ has near-constant $\theta \sim \frac{\pi}{2}$ and acquires an infinitesimal "dimple" at $\tau \sim 1$ similar to the $O(A)$ dimple in the $dS_3$ surface (3.22). It then joins an equivalent surface in the past universe. The full connected surface stretching from $I^+$ to $I^-$ thus has a constriction at the neck (Fig. 3) and is not smooth. In the absence of the detailed solution, it is difficult to check if the $\theta' = 0$ surface at $\theta = \frac{\pi}{2}$ has minimal area although the area integral (3.19) is identical to (3.12), (3.13).

## 4. Discussion

We have seen that 4-dim de Sitter entropy $\frac{l^2 V_{S^2}}{4G_4} = \frac{\pi l^2}{G_4}$ which is the area of the cosmological event horizon for regions $N$ and $S$ in the static patch coordinatization (Fig. 2) arises as the coefficient of the divergent area $\frac{\pi l^2}{G_4}\frac{1}{\epsilon}$ of certain codim-2 real timelike extremal surfaces. These wrap an $S^1$ and stretch in the bulk time direction from the future boundary $I^+$ in $F$ to the past boundary $I^-$ in $P$, the areas along the $S^1$ and the time direction compensating for $V_{S^2}$. These surfaces all lie in a boundary Euclidean time slice of the bulk space, either (i) in some equatorial plane of the $S^2$, where they exclude the regions behind the horizons, or (ii) on the $w = const$ slice. They all pass through the bifurcation region (with only the divergent term): the ones in the equatorial planes can be seen to have minimal area. The bifurcation region behaves a bit like $AdS$ with regard to area extremization. These surfaces are in some sense rotated versions of surfaces of Hartman and Maldacena [19] in the $AdS$ black hole (which itself after a rotation resembles the present de Sitter static coordinatization).

The restriction to a boundary Euclidean time slice which encodes a symmetry direction gives codim-2 surfaces, consistent with the $\frac{l^2}{G_4}$ scaling of de Sitter entropy. The fact that the divergence coefficient arises independent of which particular boundary Euclidean time slice is used suggests that there exists some formulation which makes manifest this independence on the particular slice. The boundary Euclidean time slice is of course reminiscent of the constant time slice containing spatial subsystems in the usual formulation of entanglement entropy, which we will elaborate on below.

In the context of $dS/CFT$ [7–9], de Sitter space is conjectured to be dual to a hypothetical Euclidean non-unitary CFT that lives on the future boundary $\mathcal{I}^+$, with the dictionary $\Psi_{dS} = Z_{CFT}$ [9], where $\Psi_{dS}$ is the late-time Hartle–Hawking wavefunction of the universe with appropriate boundary conditions and $Z_{CFT}$ the dual CFT partition function. The dual CFT$_d$ energy–momentum tensor correlators reveal central charge coefficients $\mathcal{C}_d \sim i^{1-d}\frac{l^{d-1}}{G_{d+1}}$ in $dS_{d+1}$ (effectively analytic continuations from $AdS/CFT$). This is real and negative in $dS_4$ so that $dS_4/CFT_3$ is reminiscent of ghost-like non-unitary theories. In [24], a higher spin $dS_4$ duality was conjectured involving a 3-dim CFT of anti-commuting $Sp(N)$ (ghost) scalars, studied previously in [25,26] (see also e.g. [27–32]).

As we have seen, the areas of the codim-2 extremal surfaces here scale as $\frac{l^{d-1}}{G_{d+1}}$ but have a different numerical factor in other dimensions: perhaps this is not unexpected since $dS/CFT$ away from $dS_4$ appears more exotic. Relatedly in $dS_4$, interpreting the extremal surface area as an area law divergence in a dual CFT, one might worry about the detailed significance of the coefficient: rescaling the ultraviolet cutoff changes the precise coefficient. The bulk surface stretches from the future boundary $I^+$ regulated at $\epsilon = \frac{\epsilon_c}{l}$ (expressed in terms of the de Sitter scale $l$), and passes through the bifurcation region at $\tau = 1$ (which contains the turning point) and its area is unambiguous however. Perhaps it is noteworthy that in the limit of the subregion being the full space, the surface in question almost cloaks the horizons suggesting that the area in some sense encodes degrees of freedom behind the horizons (although these are Cauchy horizons for the future/past universes).

In the static patch coordinatization here, since the boundary at $I^\pm$ is Euclidean $R_w \times S^{d-1}$, it is reasonable to imagine the dual to de Sitter space to comprise two copies of the dual Euclidean nonunitary CFT on a cylindrical Euclidean space of the form $R_w \times S^{d-1}$. Noting de Sitter entropy, one might be tempted to regard it as an "entangled state" of $CFT_F \times CFT_P$ i.e. two copies of the dual CFT, with de Sitter entropy appearing as the coefficient of some "generalized entanglement entropy". This cannot be entanglement in the usual sense since the dual CFTs are Euclidean: however the presence of a translation symmetry along some boundary direction taken as Euclidean time allows formulating a generalized entanglement in a formal manner along the usual lines. The connected extremal surfaces here (Fig. 2) stretching from $CFT_F$ at $I^+$ to $CFT_P$ at $I^-$ appear to corroborate this interpretation.[2] The negative central charge of $dS_4/CFT_3$ suggests that $CFT_{F,P}$ are akin to ghost-CFTs, as mentioned above.

With a view to elaborating further, we first recall that certain complex codim-2 extremal surfaces were found to give negative areas in $dS_4$ [14,15], consistent with the negative central charge (amounting to analytic continuation from Ryu–Takayanagi in $AdS$). Towards gaining some insight on generalizations of entanglement entropy to ghost-like theories and negative entanglement, certain investigations were carried out in [16] in toy 2-dim ghost-CFTs using the replica formulation (giving $S < 0$ for $c < 0$ ghost-CFTs under certain conditions) and in quantum mechanical toy models of "ghost-spins" (reviewed briefly in Appendix B) via reduced density matrices. A single ghost-spin is defined as a 2-state spin variable with indefinite inner product $\langle\uparrow \mid \uparrow\rangle = 0 = \langle\downarrow \mid \downarrow\rangle$ and $\langle\uparrow \mid \downarrow\rangle = 1 = \langle\downarrow \mid \uparrow\rangle$, akin to the inner products in the $bc$-ghost system (in contrast, a single spin has $\langle\uparrow \mid \uparrow\rangle = 1 = \langle\downarrow \mid \downarrow\rangle$). Then the states $|\pm\rangle = \frac{1}{\sqrt{2}}(|\uparrow\rangle \pm |\downarrow\rangle)$ satisfy $\langle\pm|\pm\rangle = \pm 1$. A two ghost-spin state then has norm

[2] From [9], the $CFT$ partition function $Z_{CFT} = \Psi_{dS} \sim e^{iI_{dS}}$ has imaginary pieces in a semiclassical expansion: however bulk expectation values involve the probability $|\Psi_{dS}|^2 = \Psi^*_{dS}\Psi_{dS}$ where these cancel, which also might be taken to point to $CFT_F \times CFT_P$ for bulk physics.

$$|\psi\rangle = \psi^{\alpha\beta}|\alpha\beta\rangle: \quad \langle\psi|\psi\rangle = \gamma_{\alpha\kappa}\gamma_{\beta\lambda}\psi^{\alpha\beta}\psi^{\kappa\lambda *}\,,$$
$$\gamma_{++} = 1, \;\; \gamma_{--} = \langle -|-\rangle = -1\,, \tag{4.1}$$

where $\gamma_{\alpha\beta}$ is the indefinite metric. Thus although states $|-\rangle$ have negative norm, the state $|-\rangle|-\rangle$ has positive norm. Ensembles of ghost-spins were developed further in [17] for entanglement properties. In [18] certain 1-dim ghost-spin chains with specific nearest-neighbour interactions were found to yield $bc$-ghost CFTs in the continuum limit. Some ongoing work deals with certain $N$-level generalizations of the 2-level ghost-spins above. In this light, one might regard appropriate 3-dimensional $N$-level ghost-spin chains as approximating the ghost-$CFT_3$s above and thereby possibly $dS_4$ with $\frac{l^2}{G_4} \sim N$ (the negative central charge suggests $dS_4$ is like a ghost-CFT more generally, not just in the higher spin context of [24]). Thinking thereby of appropriate 3-dim ghost-spin systems as microscopic realizations in the same universality class as ghost-CFTs dual to $dS_4$, we can study entanglement properties for states in the ghost-spin system. Then consider an entangled state of the form

$$|\psi\rangle = \sum \psi^{i_n^F, i_n^P}|i_n^F\rangle|i_n^P\rangle \tag{4.2}$$

where $\psi^{i_n^F, i_n^P}$ are coefficients entangling a generic ghost-spin configuration $|i_n^F\rangle$ from $CFT_F$ at $I^+$ with an identical one $|i_n^P\rangle$ from $CFT_P$ at $I^-$. (Entangled states of this schematic form appear in [27]: the state (4.2) however involves entanglement between states of ghost-spin systems, or ghost-CFTs.) The state (4.2) is akin to a correlated ghost-spin state with an even number of ghost-spins, as discussed in [17,18]. It necessarily has positive norm,

$$\sum_{i_n^F, i_n^P} \gamma_{i_n^F, i_n^F}\,\gamma_{i_n^P, i_n^P}\,\psi^{i_n^F, i_n^P}\left(\psi^{i_n^F, i_n^P}\right)^* \xrightarrow{F\equiv P} \sum_{i_n} |\psi^{i_n^F, i_n^P}|^2 \tag{4.3}$$

using the form (4.1), since we are entangling identical states $i_n^F$ and $i_n^P$: thus it has positive entanglement, as in [17,18]. Since each constituent state $|i_n^{F,P}\rangle$ is $N$-level, i.e. with $N$ internal degrees of freedom, the entanglement entropy scales as $N \sim \frac{l^2}{G_4}$. The state (4.2) is akin to the thermofield double dual to the eternal $AdS$ black hole [33]. This suggests the speculation that 4-dim de Sitter space is perhaps approximately dual to $CFT_F \times CFT_P$ in the entangled state (4.2) and the generalized entanglement entropy of the latter scales as de Sitter entropy. It is also interesting to speculate about ER=EPR [34] and so on in this context[3]: the roles of bulk time evolution and boundary Euclidean time evolution are likely to make this structure somewhat different from $AdS$. We hope to explore these further.

## Acknowledgements

It is a pleasure to thank Dileep Jatkar for interesting discussions and initial collaboration on this work. I also thank Sumit Das and Sandip Trivedi for interesting conversations over the last two years, Andy Strominger for interesting conversations at SpentaFest, ICTS, and Amitabh Virmani for useful comments on a draft. This work is partially supported by a grant to CMI from the Infosys Foundation.

## Appendix A. Reviewing extremal surfaces in Poincare $dS$

Reviewing [14,15], consider de Sitter space in Poincare slicing, $ds^2 = \frac{R_{dS}^2}{\tau^2}(-d\tau^2 + dw^2 + dx_i^2)$. One of the $d$ spatial directions $w$ is regarded as boundary Euclidean time. On a $w = const$ slice, consider a strip subregion at $I^+$ with width $\Delta x = l$ and extremal surfaces anchored at the subregion boundary and dipping into the bulk towards the past. The area functional is

$$S_{dS} = \frac{1}{4G_{d+1}}\int \prod_{i=1}^{d-2}\frac{R_{dS}dy_i}{\tau}\frac{R_{dS}}{\tau}\sqrt{d\tau^2 - dx^2}$$
$$= \frac{R_{dS}^{d-1}V_{d-2}}{4G_{d+1}}\int \frac{d\tau}{\tau^{d-1}}\sqrt{1-\dot{x}^2}\,, \tag{A.1}$$

the sign under the square root reflecting real timelike surfaces. The extremization gives

$$\left(\frac{dx}{d\tau}\right)^2 \equiv \dot{x}^2 = \frac{B^2\tau^{2d-2}}{1+B^2\tau^{2d-2}}\,,$$
$$S_{dS} = \frac{R_{dS}^{d-1}}{4G_{d+1}}V_{d-2}\int_\epsilon^{\tau_0}\frac{d\tau}{\tau^{d-1}}\frac{1}{\sqrt{1+B^2\tau^{2d-2}}}\,. \tag{A.2}$$

We see that the square root in the area integral is quite different from (3.7): there is no minus sign so the behaviour is monotonic with $B$ (no turning point exists where $\dot{x}^2 \to \infty$ for real $\tau$; complex extremal surfaces with turning points exist along imaginary time paths $\tau = iT$, amounting to analytic continuation from Ryu–Takayanagi in $AdS$). The area is maximised for $B = 0$, giving maximally timelike surfaces ($\dot{x} = 0$) which simply "hang" down into the bulk. For surfaces stretching all the way to $\tau = -\infty$, the area becomes

$$S_{dS} = \frac{R_{dS}^{d-1}}{4G_{d+1}}V_{d-2}\int_{-\infty}^{-\epsilon}\frac{d\tau}{\tau^{d-1}} \;\longrightarrow\; \frac{R_{dS}^2}{4G_4}\frac{V_1}{\epsilon} \quad [dS_4]\,, \tag{A.3}$$

independent of the size of the subregion. There are no finite cutoff-independent pieces for these surfaces since those contributions die at $|\tau| \to \infty$.

Now consider spherical subregions on $\mathcal{I}^+$, with radius $l$ satisfying $0 \le r \le l$. Towards studying spherical entangling surfaces, we parametrize the spatial part of the $dS$ metric in polar coordinates. The $w = const$ slice has metric $ds^2 = \frac{R_{dS}^2}{\tau^2}(-d\tau^2 + dr^2 + r^2 d\Omega_{d-2}^2)$. The bulk codim-2 surface $r = r(\tau)$ has area functional in Planck units

$$S_{dS} = \frac{1}{4G_{d+1}}\int \prod_{i=1}^{d-2}\frac{R_{dS}rd\Omega_i}{\tau}\frac{R_{dS}}{\tau}\sqrt{d\tau^2 - dr^2}$$
$$= \frac{R_{dS}^{d-1}\Omega_{d-2}}{4G_{d+1}}\int \frac{d\tau}{\tau^{d-1}}r^{d-2}\sqrt{1-\dot{r}^2}\,. \tag{A.4}$$

The variational equation of motion for an extremum $\frac{\partial}{\partial\tau}(\frac{\partial\mathcal{L}}{\partial\dot{r}}) = \frac{\partial\mathcal{L}}{\partial r}$ leads to (with $\frac{dr}{d\tau} \equiv \dot{r}$)

$$\frac{\partial}{\partial\tau}\left(\frac{r^{d-2}}{\tau^{d-1}}\frac{\dot{r}}{\sqrt{1-\dot{r}^2}}\right) = \frac{d-2}{\tau^{d-1}}r^{d-3}\sqrt{1-\dot{r}^2}$$
$$\longrightarrow \quad r(\tau) = \sqrt{l^2+\tau^2}\,. \tag{A.5}$$

This satisfies the boundary conditions $r \to l$ as $\tau \to 0$. Unlike the strip case, there are no parameters here for $d > 2$. For $\tau$ real, there is no bulk turning point where $\dot{r} \to \infty$: instead $r^2 \to \tau^2$ asymptotically. Since $r(\tau) \ge l$, this surface bends "outwards" from the subregion boundary (all interior points within the subregion satisfy $0 \le r \le l$). This real timelike surface $\dot{r} \le 1$ does not "end" at any finite $\tau$: considering the whole $\tau$-range, we obtain

[3] I thank Juan Maldacena for an interesting correspondence in this regard.

$$S_{dS} = \frac{R_{dS}^{d-1}\Omega_{d-2} l}{4G_{d+1}} \int_{-\infty}^{-\epsilon} \frac{d\tau}{\tau^{d-1}} (l^2+\tau^2)^{(d-3)/2} \quad \xrightarrow{dS_4} \quad \frac{R_{dS}^2}{4G_4}\frac{A_1}{\epsilon} \,, \tag{A.6}$$

with $\tau_{UV} = -\epsilon$, and $A_1 = 2\pi l$ the $S^1$ interface area ($dS_4$). For $dS_5$, we obtain $S_{dS} = \frac{R_{dS}^3}{8G_5}\frac{A_2}{\epsilon^2} + \frac{\pi R_{dS}^3}{2G_5}\log\frac{l}{\epsilon}$, with $A_2 = 4\pi l^2$ the $S^2$ interface area. Again the finite pieces vanish.

## Appendix B. Reviewing ghost-spins and ghost-spin chains

Here we review ghost-spins and ghost-spin chains, based on [16–18]. A single ghost-spin is defined as a 2-state spin variable with indefinite inner product $\langle\uparrow|\uparrow\rangle = 0 = \langle\downarrow|\downarrow\rangle$ and $\langle\uparrow|\downarrow\rangle = 1 = \langle\downarrow|\uparrow\rangle$. Then $|\pm\rangle = \frac{1}{\sqrt{2}}(|\uparrow\rangle \pm |\downarrow\rangle)$ have positive/negative norm. We normalize positive/negative norm states with norm $\pm 1$ respectively. Now consider the two ghost-spin state (4.1). The full density matrix is $\rho = |\psi\rangle\langle\psi| = \sum \psi^{\alpha\beta}\psi^{\kappa\lambda *}|\alpha\beta\rangle\langle\kappa\lambda|$. Tracing over one of the ghost-spins leads to a reduced density matrix $(\rho_A)^{\alpha\kappa} = \gamma_{\beta\lambda}\psi^{\alpha\beta}\psi^{\kappa\lambda *} = \gamma_{\beta\beta}\psi^{\alpha\beta}\psi^{\kappa\beta *}$,

$$\begin{aligned}
(\rho_A)^{++} &= |\psi^{++}|^2 - |\psi^{+-}|^2 \,, \\
(\rho_A)^{+-} &= \psi^{++}\psi^{-+*} - \psi^{+-}\psi^{--*} \,, \\
(\rho_A)^{-+} &= \psi^{-+}\psi^{++*} - \psi^{--}\psi^{+-*} \,, \\
(\rho_A)^{--} &= |\psi^{-+}|^2 - |\psi^{--}|^2 \,,
\end{aligned} \tag{B.1}$$

for the remaining ghost-spin. Then $tr\rho_A = \gamma_{\alpha\kappa}(\rho_A)^{\alpha\kappa} = (\rho_A)^{++} - (\rho_A)^{--}$. Thus the reduced density matrix is normalized to have $tr\rho_A = tr\rho = \pm 1$ depending on whether the state (4.1) is positive or negative norm. The entanglement entropy calculated as the von Neumann entropy of $\rho_A$ is $S_A = -\gamma_{\alpha\beta}(\rho_A\log\rho_A)^{\alpha\beta}$, perhaps best defined in terms of a mixed-index reduced density matrix $(\rho_A)^{\alpha}{}_{\kappa}$. As an illustration, consider a simple family of states [16] with a diagonal RDM: setting $\psi^{-+*} = \psi^{+-}\psi^{--*}/\psi^{++}$ in the states (4.1) gives

$$\begin{aligned}
&(\rho_A)^{\alpha\beta}|\alpha\rangle\langle\beta| = \pm x|+\rangle\langle+| \mp (1-x)|-\rangle\langle-| \,, \\
&x = \frac{|\psi^{++}|^2}{|\psi^{++}|^2 + |\psi^{--}|^2} \quad [0<x<1], \\
&(\rho_A)^{\kappa}_{\alpha} = \gamma_{\alpha\beta}(\rho_A)^{\beta\kappa}: \quad (\rho_A)^{+}_{+} = \pm x, \qquad (\rho_A)^{-}_{-} = \pm(1-x),
\end{aligned} \tag{B.2}$$

where the $\pm$ pertain to positive/negative norm states respectively (note that $tr\rho_A = (\rho_A)^{+}_{+} + (\rho_A)^{-}_{-} = \pm 1$). The location of the negative eigenvalue is different for positive/negative norm states, leading to different results for the von Neumann entropy. Now $\log\rho_A$ simplifies to $(\log\rho_A)^{+}_{+} = \log(\pm x)$ and $(\log\rho_A)^{-}_{-} = \log(\pm(1-x))$. The entanglement entropy $S_A = -\gamma_{\alpha\beta}(\rho_A\log\rho_A)^{\alpha\beta}$ becomes $S_A = -(\rho_A)^{+}_{+}(\log\rho_A)^{+}_{+} - (\rho_A)^{-}_{-}(\log\rho_A)^{-}_{-}$ and so

$$\langle\psi|\psi\rangle \gtrless 0: \quad S_A = -(\pm x)\log(\pm x) - (\pm(1-x))\log(\pm(1-x)) \,. \tag{B.3}$$

For positive norm states, $S_A$ is manifestly positive since $x<1$, just as in an ordinary 2-spin system. Negative norm states give a negative real part for EE ($x<1$ and the logarithms are negative), and an imaginary part (the simplest branch has $\log(-1) = i\pi$).

Note that restricting to the subspace $|\psi\rangle = \psi^{++}|++\rangle + \psi^{--}|--\rangle$, we obtain solely positive norm states and positive RDM and entanglement. For ensembles with an even number of ghost-spins, such correlated ghost-spin states always exist comprising positive norm subsectors. This leads to (4.2), (4.3). Odd ghost-spins behave differently: e.g. $|\psi\rangle = \psi^{++\cdots}|++\ldots\rangle + \psi^{--\cdots}|--\ldots\rangle$ has norm $\langle\psi|\psi\rangle = |\psi^{++\cdots}|^2 + (-1)^n|\psi^{--\cdots}|^2$ and mixed-index RDM components $(\rho_A)^{+}_{+} = |\psi^{++\cdots}|^2$, $(\rho_A)^{-}_{-} = (-1)^n|\psi^{--\cdots}|^2$. This is not positive definite for $n$ odd (even if $\langle\psi|\psi\rangle > 0$). Ensembles of ghost-spins and spins also show interesting entanglement patterns [17].

It is natural to expect that infinite 1-dim chains of ghost-spins lead in a continuum limit to 2-dim ghost-CFTs, akin to the well-known fact that the Ising spin chain at criticality is described by a CFT of free massless fermions. Consider spin variables $\sigma_{bn}$, $\sigma_{cn}$ satisfying

$$\{\sigma_{bn}, \sigma_{cn}\} = 1 \,, \qquad [\sigma_{bn}, \sigma_{bn'}] = [\sigma_{cn}, \sigma_{cn'}] = [\sigma_{bn}, \sigma_{cn'}] = 0 \,, \tag{B.4}$$

which are consistent with the off-diagonal inner product between ghost-spin states. These spin variables are self-adjoint and act on two states $|\uparrow\rangle$, $|\downarrow\rangle$, at each lattice site $n$, as

$$\begin{aligned}
&\sigma_{bn}^{\dagger} = \sigma_{bn}, \ \ \sigma_{cn}^{\dagger} = \sigma_{cn} \,; \qquad \sigma_b|\downarrow\rangle = 0, \quad \sigma_b|\uparrow\rangle = |\downarrow\rangle, \\
&\sigma_c|\uparrow\rangle = 0, \quad \sigma_c|\downarrow\rangle = |\uparrow\rangle.
\end{aligned} \tag{B.5}$$

Consider now a 1-dim ghost-spin chain with nearest neighbour interaction Hamiltonian

$$H = J\sum_n \left(\sigma_{b(n)}\sigma_{c(n+1)} + \sigma_{b(n)}\sigma_{c(n-1)}\right) \,. \tag{B.6}$$

This is not quite Ising-like: in fact it describes a "hopping" type Hamiltonian, which kills an $\uparrow$-spin at site $n$ and creates it at site $n\pm 1$, so that $\uparrow_n$ hops to $\uparrow_{n\pm 1}$.

The $\sigma_{bn}, \sigma_{cn}$ above are analogous to the $b_n, c_n$ operators of the $bc$-ghost CFT, satisfying $\{b_n, c_m\} = \delta_{n+m,0}$: however $\sigma_{bn}$, $\sigma_{cn}$ are bosonic, commuting at distinct lattice sites. Fermionic ghost-spin variables constructed via a Jordan–Wigner transformation

$$a_{bn} = \prod_{k=1}^{n-1} i(1-2\sigma_{ck}\sigma_{bk})\sigma_{bn} \,, \qquad a_{cn} = \prod_{k=1}^{n-1}(-i)(1-2\sigma_{ck}\sigma_{bk})\sigma_{cn} \,, \tag{B.7}$$

give

$$\{a_{bi}, a_{cj}\} = \delta_{ij} \,, \qquad \{a_{bi}, a_{bj}\} = 0 \,, \qquad \{a_{ci}, a_{cj}\} = 0 \,. \tag{B.8}$$

Unlike the $\sigma$ spin operators, these anticommute not just at the same site $i$ but also at distinct sites $i, j$. The states satisfy $a_b|\downarrow\rangle = 0$, $a_b|\uparrow\rangle = |\downarrow\rangle$, $a_c|\uparrow\rangle = 0$, $a_c|\downarrow\rangle = |\uparrow\rangle$, $\langle\downarrow|a_b = 0$, $\langle\uparrow|a_b = \langle\downarrow|$, $\langle\downarrow|a_c = \langle\uparrow|$, $\langle\uparrow|a_c = 0$. To construct states and their inner products, we have to be careful about the ordering of the operators and the spin excitations. We adopt the convention that $\langle\uparrow\uparrow|\downarrow\downarrow\rangle = 1$, $|\overrightarrow{\uparrow\uparrow}\rangle = a_{c1}a_{c2}|\downarrow\downarrow\rangle$, $\langle\overleftarrow{\downarrow\downarrow}| = \langle\uparrow\uparrow|a_{b2}a_{b1}$, giving $\langle\overleftarrow{\downarrow\downarrow}|\overrightarrow{\uparrow\uparrow}\rangle = 1$, illustrating two fermionic ghost-spins. The underlining right arrow in the ket displays the order of the operator excitations to be increasing to the right; the underlining left arrow in the bra shows the order as increasing to the left. Then a state $\psi_1|\downarrow\downarrow\rangle + \psi_2|\overrightarrow{\uparrow\uparrow}\rangle$ gives $\psi_1^*\psi_2\langle\uparrow\uparrow|a_{b_2}a_{b1}\ a_{c1}a_{c2}|\downarrow\downarrow\rangle + \psi_2^*\psi_1\langle\uparrow\uparrow|\downarrow\downarrow\rangle = \psi_1^*\psi_2 + \psi_2^*\psi_1$, the expected indefinite norm.

In terms of the fermionic ghost-spin variables, the Hamiltonian (B.6) becomes

$$H \ \to \ iJa_{bn}(a_{c(n+1)} - a_{c(n-1)}) \ \sim \ -b\partial c \,, \tag{B.9}$$

which is the lattice discretization of the $bc$-ghost CFT. Using momentum space variables $b_k = \frac{1}{\sqrt{N}} \sum_n e^{ikn} a_{bn}$, $c_k = \frac{1}{\sqrt{N}} \sum_n e^{ikn} a_{cn}$, we obtain $\{b_k, c_{k'}\} = \delta_{k+k',0}$, $\{b_k, b_{k'}\} = 0 = \{c_k, c_{k'}\}$. Reinstating the lattice spacing $a$, we obtain in the continuum limit $a \to 0$

$$H = 2J \sum_k \sin(k'a)\, b_k c_{k'}\, \delta_{k+k',0} = 2Ja \sum_k k b_{-k} c_k \xrightarrow{J\sim 1/2a} \sum_{k>0} k \left(b_{-k} c_k + c_{-k} b_k\right) + \zeta \,, \tag{B.10}$$

with $\zeta$ the normal ordering constant giving the zero point energy. The scaling $J \sim \frac{1}{2a}$ ensures that the nearest neighbour lattice interaction leads to a nontrivial continuum interaction. Consider now the symmetries of the ghost-spin chain Hamiltonian (B.6): first, the phase rotation symmetry $\sigma_{b(n)} \to e^{i\alpha} \sigma_{b(n)}$, $\sigma_{c(n+1)} \to e^{-i\alpha} \sigma_{c(n+1)}$, is the microscopic reflection of the $U(1)$ symmetry in the continuum $bc$-CFT. Also

$$a \to \xi^{-1} a \,, \quad H \to \xi H \,, \qquad \sigma_{b(n)} \to \xi^{\lambda} \sigma_{b(n)} \,, \quad \sigma_{c(n+1)} \to \xi^{1-\lambda} \sigma_{c(n+1)} \,, \tag{B.11}$$

is a global scaling symmetry of the ghost-spin variables $(\sigma_b, \sigma_c)$ for any constant $\lambda$: this underlies the conformal symmetry of the $bc$-CFT, with conformal weights $(h_b, h_c) = (\lambda, 1-\lambda)$. Further details appear in [18]. This suggests that ghost-spins are microscopic building blocks of ghost-like CFTs in general, including 3-dim ones.

## References


[1] G.W. Gibbons, S.W. Hawking, Cosmological event horizons, thermodynamics, and particle creation, Phys. Rev. D 15 (1977) 2738, https://doi.org/10.1103/PhysRevD.15.2738.

[2] lM. Spradlin, A. Strominger, A. Volovich, Les Houches lectures on de Sitter space, arXiv:hep-th/0110007.

[3] J.M. Maldacena, The large N limit of superconformal field theories and supergravity, Adv. Theor. Math. Phys. 2 (1998) 231, Int. J. Theor. Phys. 38 (1999) 1113, arXiv:hep-th/9711200.

[4] S.S. Gubser, I.R. Klebanov, A.M. Polyakov, Gauge theory correlators from noncritical string theory, Phys. Lett. B 428 (1998) 105, arXiv:hep-th/9802109.

[5] E. Witten, Anti-de Sitter space and holography, Adv. Theor. Math. Phys. 2 (1998) 253, arXiv:hep-th/9802150.

[6] O. Aharony, S.S. Gubser, J.M. Maldacena, H. Ooguri, Y. Oz, Large N field theories, string theory and gravity, Phys. Rep. 323 (2000) 183, arXiv:hep-th/9905111.

[7] A. Strominger, The dS / CFT correspondence, J. High Energy Phys. 0110 (2001) 034, arXiv:hep-th/0106113.

[8] E. Witten, Quantum gravity in de Sitter space, arXiv:hep-th/0106109.

[9] J.M. Maldacena, Non-Gaussian features of primordial fluctuations in single field inflationary models, J. High Energy Phys. 0305 (2003) 013, arXiv:astro-ph/0210603.

[10] S. Ryu, T. Takayanagi, Holographic derivation of entanglement entropy from AdS/CFT, Phys. Rev. Lett. 96 (2006) 181602, arXiv:hep-th/0603001.

[11] S. Ryu, T. Takayanagi, Aspects of holographic entanglement entropy, J. High Energy Phys. 0608 (2006) 045, arXiv:hep-th/0605073.

[12] V.E. Hubeny, M. Rangamani, T. Takayanagi, A covariant holographic entanglement entropy proposal, J. High Energy Phys. 0707 (2007) 062, arXiv:0705.0016 [hep-th].

[13] M. Rangamani, T. Takayanagi, Holographic entanglement entropy, Lect. Notes Phys. 931 (2017) 1, https://doi.org/10.1007/978-3-319-52573-0, arXiv:1609.01287 [hep-th].

[14] K. Narayan, De Sitter extremal surfaces, Phys. Rev. D 91 (12) (2015) 126011, https://doi.org/10.1103/PhysRevD.91.126011, arXiv:1501.03019 [hep-th].

[15] K. Narayan, De Sitter space and extremal surfaces for spheres, Phys. Lett. B 753 (2016) 308, https://doi.org/10.1016/j.physletb.2015.12.019, arXiv:1504.07430 [hep-th].

[16] K. Narayan, On $dS_4$ extremal surfaces and entanglement entropy in some ghost CFTs, Phys. Rev. D 94 (4) (2016) 046001, https://doi.org/10.1103/PhysRevD.94.046001, arXiv:1602.06505 [hep-th].

[17] D.P. Jatkar, K. Narayan, Entangled spins and ghost-spins, Nucl. Phys. B 922 (2017) 319, https://doi.org/10.1016/j.nuclphysb.2017.07.002, arXiv:1608.08351 [hep-th].

[18] D.P. Jatkar, K. Narayan, Ghost-spin chains, entanglement and $bc$-ghost CFTs, Phys. Rev. D (2017), arXiv:1706.06828 [hep-th].

[19] T. Hartman, J. Maldacena, Time evolution of entanglement entropy from black hole interiors, J. High Energy Phys. 1305 (2013) 014, https://doi.org/10.1007/JHEP05(2013)014, arXiv:1303.1080 [hep-th].

[20] D. Das, S.R. Das, K. Narayan, DS/CFT at uniform energy density and a de Sitter 'bluewall', J. High Energy Phys. 1404 (2014) 116, https://doi.org/10.1007/JHEP04(2014)116, arXiv:1312.1625 [hep-th].

[21] S. Hawking, J.M. Maldacena, A. Strominger, De Sitter entropy, quantum entanglement and AdS / CFT, J. High Energy Phys. 0105 (2001) 001, https://doi.org/10.1088/1126-6708/2001/05/001, arXiv:hep-th/0002145.

[22] K. Nguyen, De Sitter-invariant states from holography, arXiv:1710.04675 [hep-th].

[23] K. Narayan, T. Takayanagi, S.P. Trivedi, AdS plane waves and entanglement entropy, J. High Energy Phys. 1304 (2013) 051, https://doi.org/10.1007/JHEP04(2013)051, arXiv:1212.4328 [hep-th].

[24] D. Anninos, T. Hartman, A. Strominger, Higher spin realization of the dS/CFT correspondence, arXiv:1108.5735 [hep-th].

[25] A. LeClair, Quantum critical spin liquids, the 3D Ising model, and conformal field theory in $2+1$ dimensions, arXiv:cond-mat/0610639.

[26] A. LeClair, M. Neubert, Semi-Lorentz invariance, unitarity, and critical exponents of symplectic fermion models, J. High Energy Phys. 0710 (2007) 027, https://doi.org/10.1088/1126-6708/2007/10/027, arXiv:0705.4657 [hep-th].

[27] R. Bousso, A. Maloney, A. Strominger, Conformal vacua and entropy in de Sitter space, Phys. Rev. D 65 (2002) 104039, https://doi.org/10.1103/PhysRevD.65.104039, arXiv:hep-th/0112218.

[28] V. Balasubramanian, J. de Boer, D. Minic, Notes on de Sitter space and holography, Class. Quantum Gravity 19 (2002) 5655, Ann. Phys. 303 (2003) 59, arXiv:hep-th/0207245.

[29] D. Harlow, D. Stanford, Operator dictionaries and wave functions in AdS/CFT and dS/CFT, arXiv:1104.2621 [hep-th].

[30] G.S. Ng, A. Strominger, State/operator correspondence in higher-spin dS/CFT, Class. Quantum Gravity 30 (2013) 104002, arXiv:1204.1057 [hep-th].

[31] D. Das, S.R. Das, A. Jevicki, Q. Ye, Bi-local construction of Sp(2N)/dS higher spin correspondence, J. High Energy Phys. 1301 (2013) 107, arXiv:1205.5776 [hep-th].

[32] D. Anninos, F. Denef, D. Harlow, The wave function of Vasiliev's universe – a few slices thereof, Phys. Rev. D 88 (2013) 084049, arXiv:1207.5517 [hep-th].

[33] J.M. Maldacena, Eternal black holes in anti-de Sitter, J. High Energy Phys. 0304 (2003) 021, https://doi.org/10.1088/1126-6708/2003/04/021, arXiv:hep-th/0106112.

[34] J. Maldacena, L. Susskind, Cool horizons for entangled black holes, Fortschr. Phys. 61 (2013) 781, arXiv:1306.0533 [hep-th].